Chinese Chemical Letters 35 (2024) 109275

Contents lists available at ScienceDirect

Chinese Chemical Letters

journal homepage: www.elsevier.com/locate/cclet

# Programmable double-unlock nanocomplex self-supplies phenylalanine ammonia-lyase for precise phenylalanine deprivation of tumors

Chunqing Ou[a,1], Meijia Xiao[a,1], Xinyue Zheng[a,1], Xianzhou Huang[a], Suleixin Yang[b], Yingying Leng[a], Xiaowei Liu[a], Xiuqi Liang[a], Linjiang Song[c], Yanjie You[d], Shaohua Yao[a,*], Changyang Gong[a,*]

[a] Department of Biotherapy, Cancer Center and State Key Laboratory of Biotherapy, West China Hospital, Sichuan University, Chengdu 610041, China
[b] State Key Laboratory of Quality Research in Chinese Medicine, Institute of Chinese Medical Sciences, University of Macau, Avenida da Universidade, Taipa, Macau 999087, China
[c] School of Medical and Life Sciences, Chengdu University of Traditional Chinese Medicine, Chengdu 611137, China
[d] Department of Gastroenterology, People's Hospital of Ningxia Hui Autonomous Region, Yinchuan 750002, China

ARTICLE INFO

*Article history:*
Received 19 July 2023
Revised 1 November 2023
Accepted 2 November 2023
Available online 9 November 2023

*Keywords:*
Programmable double-unlock
Essential amino acids deprivation
Phenylalanine ammonia-lyase
Self-supply
Gene therapy

ABSTRACT

Essential amino acids (EAAs) deprivation is a potential antitumor approach because EAAs are critical for tumor growth. To efficiently inhibit tumor growth, continuous deprivation of EAAs is required, however, continuous deprivation without precise control will introduce toxicity to normal cells. Herein, a programmable double-unlock nanocomplex (ROCK) was prepared, which could self-supply phenylalanine ammonia-lyase (PAL) to tumor cells for phenylalanine (Phe) deprivation. ROCK was double-locked in physiological conditions when administered systemically. While ROCK actively targeted to tumor cells by integrin $\alpha v\beta 3/5$ and CD44, ROCK was firstly unlocked by cleavage of protease on tumor cell membrane, exposing CendR and R8 to enhance endocytosis. Then, hyaluronic acid was digested by hyaluronidase overexpressed in endo/lysosome of tumor cells, in which ROCK was secondly unlocked, resulting in promoting endo/lysosome escape and PAL plasmid (pPAL) release. Released pPAL could sustainably express PAL in host tumor cells until the self-supplied PAL precisely and successfully deprived Phe, thereby blocking the protein synthesis and killing tumor cells specifically. Overall, our precise Phe deprivation strategy effectively inhibited tumor growth with no observable toxicity to normal cells, providing new insights to efficiently remove intratumoral nutrition for cancer therapy.



Abundant amino acids (AA) are necessary for vigorous protein synthesis that accommodate rapid tumor growth, so AA deprivation can impede tumor growth [1–5]. Currently, most AAs deprivation strategies focus on blocking transportation [6,7] or preventing recycling of non-essential AAs [8,9]. To block the transportation, small molecular inhibitors [10], antagonists [11], or macromolecular proteinases [12] are applied, which hinder the function of non-essential AAs-associated transporter proteins. To block the recycling of non-essential AAs, relative synthetases or hydrolases are inhibited [13] or hydrolyzed [14]. However, above mentioned method could not fully eliminate the supplement of non-essential AAs because of the existence of compensatory mechanisms, such as reductive amination and transamination [15].

Different from non-essential AAs, essential AAs (EAAs) have no compensatory pathway and can only be obtained from the daily diet. Therefore, depriving EAAs is more advantageous compared with depriving non-essential AAs. Phenylalanine (Phe), one of the aromatic EAAs, is the only resource of tyrosine (Tyr) re-synthesis [16,17]. Depriving Phe may simultaneously decrease the concentration of Phe and Tyr. Phe can be specifically hydrolyzed by phenylalanine ammonia-lyase (PAL), generating nontoxic trans-cinnamic acid, rendering Phe deprivation by PAL to be a promising antitumor approach [18–20]. However, apart from tumor cells, Phe is essential to normal cells as well, which may lead to serious systemic toxicity of non-controlled PAL delivery strategy [21]. Furthermore,

* Corresponding authors.
*E-mail addresses:* shaohuayao@scu.edu.cn (S. Yao), chygong14@163.com (C. Gong).
[1] These authors contributed equally to this work.

https://doi.org/10.1016/j.cclet.2023.109275
1001-8417/

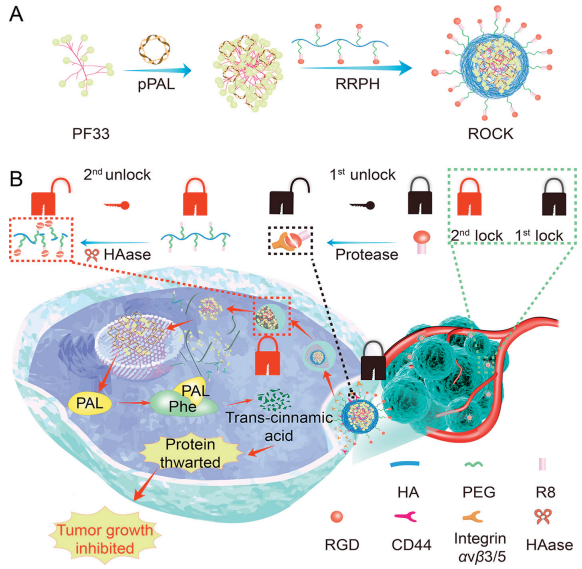


**Fig. 1.** Schematic representation of ROCK for EAAs eliminate cancer therapy. (A) The self-assembled ROCK. (B) Schematic diagram showing that ROCK was unlocked by cancer cells to deprive EAAs achieve inhibiting tumor growth.

to guarantee curative effect, continuous deprivation is required so that no chance of recovery is given to tumor cells. Therefore it is a key issue that PAL is precisely delivered and sustainably supplied in tumor cells to deprive Phe in the tumor cells without affecting normal cells.

Gene therapy can meet the requirement of sustainable and precise deprivation of Phe with a rationally designed delivery system [22–24]. To deliver the gene, viral vectors and non-viral vectors are most universally applied. Compared with viral vectors, non-viral vectors exhibit facilitated manufacture capacity, controllable structure, improved safety, and limited immunogenicity, making it a preferable choice to precisely deliver PAL gene into tumor cells to deprive Phe [25–27]. Importantly, once precisely delivered, PAL gene can be repeatedly expressed through the mechanism of transcript and translation in host tumor cells to sustainably supply PAL for Phe deprivation until tumor cells die.

Hence, we here constructed a programmable double-unlock nanocomplex (ROCK) to PAL specifically in tumor cells for sustained precise Phe deprivation to mitigate systemic toxicity (Fig. 1). To achieve precise deprivation, ROCK was locked under the physical condition after intravenous administration. Once arginine-glycine-aspartic acid (RGD) peptide and sodium hyaluronate (HA) actively escorted ROCK to tumor tissue by recognizing $\alpha v\beta 3/5$ and CD44 on tumor cell membrane [28–30], ROCK was firstly unlocked when RGD was cleaved proteolytically by protease, a cell-surface-associated protease, exposing C-end rule (CendR) and R8 to facilitate endocytosis [31–33]. After endocytosis mediated by hyaluronic acid, CendR and R8, ROCK entered the endosomal and was secondly unlocked while HA was digested by hyaluronidase (HAase), exposing the positively charged nanocomplexes. The exposed cargo, the positively charged nanocomplexes, then successfully escaped from endosome. As soon as the cargo was conveyed into cell nucleus, PAL was self-supplied through repetitious and continuous translation to hydrolyze Phe precisely in tumor cells to block the protein synthesis, the important nutrition for proliferation of tumor cells. Consequently, tumor growth was efficiently inhibited without any detected systemic toxicity. Our strategy brings new insights into precise deprivation of intratumoral nutrition for cancer therapy.

First of all, the ROCK comprised plasmids, cationic polymers, and anionic polymers. The cationic polymer, fluorinated PEI 1.8 K,

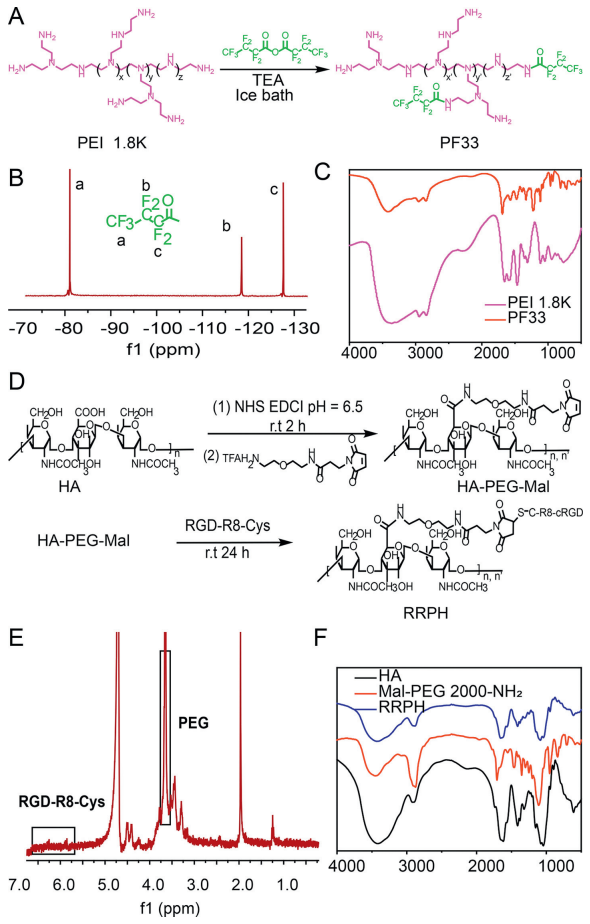


**Fig. 2.** Synthesis and characterization of PF33 and RRPH. (A) The synthesis procedure of PF33. (B) $^{19}$F NMR and (C) FT-IR of PF33. (D) The synthesis procedure of RRPH. (E) $^{1}$H NMR and (F) FT-IR of RRPH.

was successfully synthesized from PEI 1.8 K and heptafluorobutyric anhydride by one step amide reaction (Fig. 2A) and characterized *via* $^{19}$F-nuclear magnetic resonance spectra ($^{19}$F NMR) (Fig. 2B) and Fourier transform infrared spectroscopy (FT-IR) (Fig. 2C). From $^{19}$F NMR, the shifts of different C-F bounds could be seen. $^{19}$F NMR (400 MHz, $D_2O$): $\delta$ −81.07 (t, $J$ = 8.7 Hz, 3F), −118.52 (q, $J$ = 8.6 Hz, 2F), −127.61 (2F). In FT-IR spectrum, the characteristic absorption peaks of amide bonds (1686 $cm^{-1}$) and C-F (1225 $cm^{-1}$) appeared. The anionic polymer, RGD-R8 peptide-polyethylene glycol (PEG)-HA (RRPH) was successfully synthesized by amide reaction and Michael reaction (Fig. 2D) and characterized *via* $^{1}$H NMR (Fig. 2E) and FT-IR (Fig. 2F). In Fig. 2F, RRPH had three characteristic absorption peaks of raw materials, carboxyl group: 3442 $cm^{-1}$, ether bond: 1162 and 1075 $cm^{-1}$, guanidine group: 1636 $cm^{-1}$.

After the material was successfully synthesized, the ability of the polymer to condense the plasmid plays a crucial role in the efficient delivery of the plasmid. Through gel retardation assays, the ability of PF33 to condense with PAL plasmid (pPAL) was evaluated. At weight ratios greater than 1:1 (PF33:pPAL), as seen in Fig. S1 (Supporting information), PF33 demonstrated excellent plasmid condensation capability. Importantly, the plasmid in ROCK was also retarded well, which indicated that negative RRPH did not impact the condensation capability of PF33 for pPAL. In other words, ROCK met the primary requirements as a gene delivery system, and ROCK had the potential of protecting DNA from the surrounding environment. As shown in Figs. 3A and B, at a mass ratio of 1:10 (PF33:pPAL), the PF33/pPAL binary complexes displayed a hydrodynamic particle size of 81 ± 3 nm. When PF33/pPAL bi-

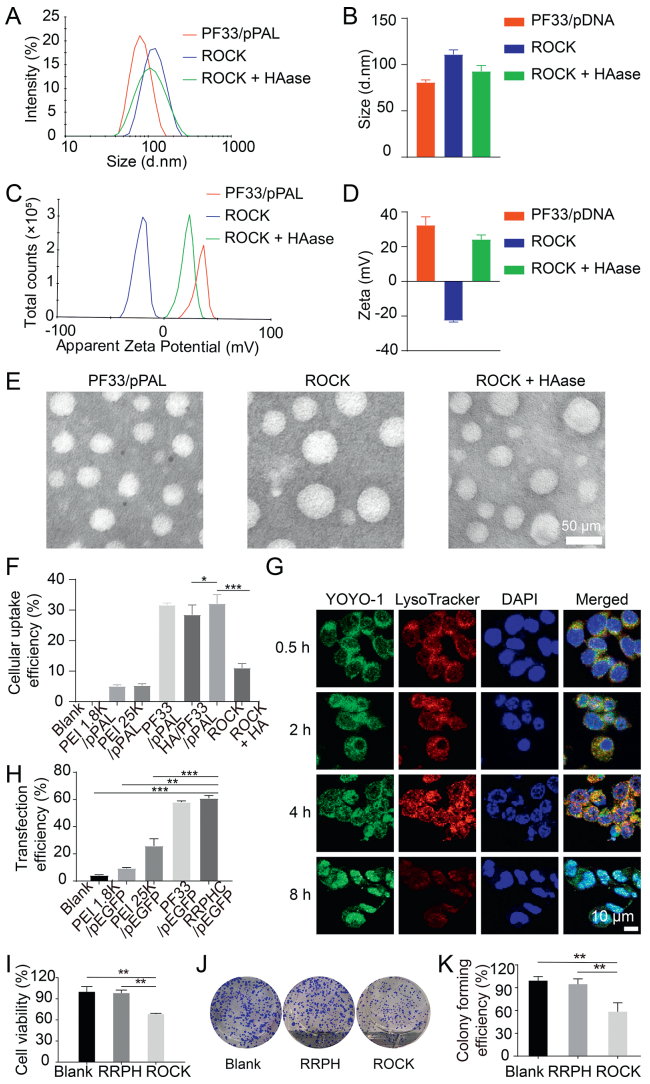


**Fig. 3.** Characterization of PF33/pPAL and ROCK and the antitumor efficiency of ROCK *in vitro*. (A, B) Size distribution and (C, D) zeta potential of PF33/pPAL, ROCK and ROCK with HAase were measured by Malvern Zetasizer. (E) morphology of PF33/pPAL, ROCK and ROCK with HAase. Scale bar: 50 nm. (F) The statistical graph of cellular uptake efficiency, $^{*}P < 0.05$, $^{**}P < 0.01$, $^{***}P < 0.005$. (G) Intracellular distribution of ROCK in HCT-116 cell at 0.5, 2, 4, and 8 h. Lysosome were strained with LysoTracker Red, pPAL plasmid was strained with YOYO-1 and cell nucleus was strained with DAPI. Scale bar: 10 μm. (H) The statistical graph of transfection efficiency was quantitatively evaluated through FCM. (I) The cell viability of HCT-116 cells after treatment with RRPH and ROCK. (J) Image of plate clone formation assay. (K) Statistical graph of colony forming efficiency. Data points represent mean ± standard deviation (SD) ($n = 3$).

nary complexes were coated with RRPH successfully, the hydrodynamic particle size of ROCK became bigger. ROCK co-incubated with HAase, a hydrodynamic particle size of ROCK was reduced from 111 ± 5 nm to 92 ± 6 nm. Figs. 3C and D showed that the surface of PF33/pPAL was positively charged, and ROCK was negatively charged. It is important that the surface charge of ROCK reversed from negative to a positive charge comparable to that of PF/pPAL when ROCK was co-incubated with HAase. Meanwhile, the spheroid morphology of PF33/pPAL, ROCK and ROCK with HAase were revealed by transmission electron microscope (TEM) images, and the variation in particle size of all three nanocomplexes is consistent with the variation in hydrated particle size (Fig. 3E). All results suggested that HAase was the first key of ROCK for precise phenylalanine deprivation in tumor cells.

Next, the toxicity of non-viral gene vectors is an important feature that determines their application. The cytotoxicity of PF33 and RRPH was determined by employing MTT assay. Compared with commercial transfer agent PEI 25 K, PF33 was confirmed with lower toxicity, even lower than PEI 1.8 K which was recognized as low-toxic material (Fig. S2A in Supporting information). This result indicated that fluorination did not introduce extra cytotoxicity, but reduced cytotoxicity of PEI 1.8 K as well. It might be due to the hydrolipidic amphiphilicity of fluorine atoms. Most importantly, RRPH which acted as the outermost layer of ROCK to go through various physicochemical and physiological conditions did not show any cytotoxicity (Fig. S2B in Supporting information). The low toxicity of PF33 and RRPH suggested that ROCK had the potential for application *in vitro* and *in vivo*.

The cellular uptake efficiency of nanocomplex for delivering genes reflects their potential for transfection in cells and the rationality of initial material design. Here, pPAL was pre-labelled with YOYO-1. As shown in Fig. 3F and Figs. S3A and B (Supporting information), compared with PEI 1.8 K/pPAL and commercial transfection PEI 25 K/pPAL, the cellular uptake efficiency of PF33/pPAL was prominently higher. Notably, after being coated with RRPH, the negatively charged ROCK exhibited comparable efficiency to the positively charged PF33/pPAL. Importantly, when the CD44 receptor of HCT-116 cells was blocked by HA, the cellular uptake efficiency of ROCK was steep. This result further showed that ROCK had the targeting capability for tumor cells. Fig. S3C (Supporting information) directly showed the cellular uptake of ROCK after 2 h. In Fig. 2G, the labelled ROCK was observed in the HCT-116 cells through confocal laser scanning microscope (CLSM). These results illustrated that RRPH could reverse the vector charge without reducing the uptake efficiency of nanocomplexes in HCT-116 cells. The entrance of ROCK to tumor cell was not impeded after coating with negatively charged RRPH, possibly due to the strong affinity of RGD-R8 and HA with integrin $\alpha v\beta 3$ receptor and CD44 on the tumor cell membrane.

We investigated the intracellular distribution and nuclear localization capacity of RRPHC in HCT-116 cells by CLSM. Briefly, HCT-116 cells were treated with ROCK loaded with YOYO-1 labeling pPAL for a determined time interval of 0.5, 2, 4, and 8 h. As shown in Fig. 3G and Fig. S4 (Supporting information), most nanocomplexes entered into cells and were entrapped in endosomes/lysosomes as the yellow which were the green fluorescence overlapped with the red at 0.5 h. Just a small part of complexes gathered around cell membranes at 0.5 h. At 2 h, the majority was localized in endosomes/lysosomes. When ROCK was given for 4 h, RRPH was broken down in endosome/lysosome by HAase releasing PF33/pPAL. At the same time, the PEI components of PF33 were protonated by $H^+$ through the "proton sponge" swelling endosomes/lysosomes and releasing PF33/pPAL from endo/lysosomes. The PF33/pPAL escaping from endosomes/lysosome further targeted cell nuclei and delivered pPAL intranuclearly as the green fluorescence overlapped with the blue exhibiting white dots at 4 h. By 8 h, all plasmids were concentrated in the nucleus displaying the obvious white areas in the images. These results suggested that ROCK could escape from endosomes/lysosomes and deliver pPAL to the cellular nucleus effectively.

*In vitro* transfection assays of PF33/pEGFP and RRPH/PF33/pEGFP had been performed on HCT-116 cell lines. As control groups, PEI 25 K/pEGFP and PEI 1.8 K/pEGFP nanocomplexes were prepared. Fig. 3H and Fig. S5 (Supporting information) turned out that RRPH/PF33/pEGFP exhibited the highest transfection efficiency at 24 h. ROCK was slightly higher than that of PF33/pEGFP and much higher than those of PEI 25 K/pEGFP (26.2% ± 4.6%, $P < 0.005$) and PEI 1.8 K/pEGFP (9.4% ± 0.6%, $P < 0.005$). The MFI data drew a similar conclusion that PF33/pEGFP displayed excellent transfection efficacy. The exciting transfection

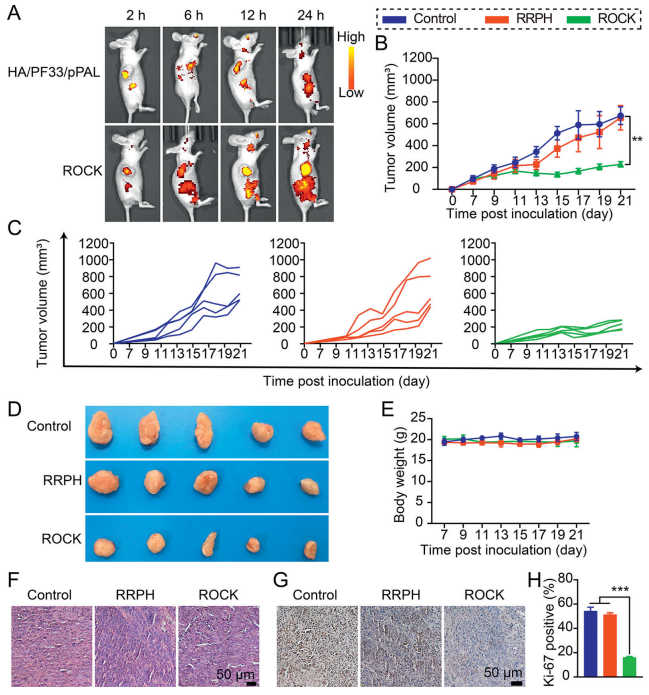


**Fig. 4.** Therapeutic efficiency *in vivo*. (A) Images of fluorescence *in vivo* that HCT-116 tumor nude mice administrated HA/PF33/pPAL or ROCK which pPAL plasmid was labelled by TOTO-3 by tail intravenous injection after 2, 6, 12, and 24 h. (B) The mean tumor growth curves and (C) mice's individual tumor growth curves with different treatments. Data points represent mean ± SD ($n = 5$). (D) The photographs and (E) the body weight splines of mice in each group after different treatments ($n = 5$). (F) H&E and (G) Ki-67 staining of tumor sections after various treatments. Scale bar: 50 μm. (H) Positive rate of Ki-67 ($n = 3$). Data points represent mean ± SD. $^{*}P < 0.05$, $^{**}P < 0.01$, $^{***}P < 0.005$.

efficiency of the negatively charged RRPH/PF33/pEGFP was shown by microscope and flow cytometry (FCM), possibly due to the advanced endosomal/lysosomal escape capability and enhanced cellular uptake caused by CD44 and integrin v3 receptor-mediated endocytosis.

The gene delivery system, RRPH/PF33/plasmid, had been confirmed that have a high transfection efficiency. We further investigated the antitumor efficiency *in vivo*. As shown in Fig. 3I, compared with the control group, the cell viability of HCT-116 was obviously reduced in the group through treatment with ROCK compared with the blank group and the group through treatment with RRPH, and ROCK was no obvious cytotoxicity for normal cells (Fig. S6 in Supporting information). The result of the plate clone formation assay was consistent with that of the MTT analysis. The number of clones was significantly decreased in the ROCK group in contrast with the control group, while treatment of RRPH had an ignorable effect on HCT-116 cell growth (Figs. 3J and K). These results suggested that Phe deprivation *via* gene therapy could inhibit the cell viability and growth of HCT-116, and have obvious antitumor efficiency *in vitro*.

Subsequently, we evaluated the tumor-targeting capacity of ROCK *in vivo*. All animal experiments strictly followed the guide for care and use of State Key Laboratory of Biotherapy approved by the Institutional Animal Care and Treatment Committee of Sichuan University. As shown in Fig. 4A, mice treated with ROCK displayed greater intensity of fluorescence in tumor tissues than those treated with HA/PF33/pPAL over a long period time (from 6 h to 24 h). Since negatively charged HA could impair the nanocomplexes' circulation within the blood and prevent accumulation in tumor tissues, as reports deemed, we attributed the surpassing tumor-targeting ability of ROCK over HA/PF33/pPAL partially to the PEG side chains which might lessen the detection and clearing of reticuloendothelial system (RES) and extend blood circulation as our previous studies validated. Compared with HA/PF33/pPAL, the increasing accumulation of ROCK in tumors owed to RGD-R8 improved tumor targeting through $\alpha v\beta 3$ receptor and cell penetration through CendR and R8.

Encouraged by the *in vitro* treatment efficacy on HCT-116 cells and biodistribution of ROCK, we further evaluated the anticancer ability of ROCK in the subcutaneous xenograft tumor model of HCT-116 colorectal carcinoma. In the period of treatment, tumors of the ROCK group grew obviously slower than all the others (Figs. 4B and C). After treatment, the tumor volumes of mice administered with ROCK were the smallest in contrast with those of control and RRPH (Fig. 4D). The body weight in the ROCK group of the mice did not show significant changes during the treatment period (Fig. 4E). All results consistently indicated that ROCK remarkably inhibited the growth of colorectal carcinoma.

Subsequently, tumor tissues were stained by hematoxylin and eosin staining (H&E) to observe the morphologies of tumor tissues and further assessed the antitumor activities. As presented in Fig. 4F, the nucleus of tumor tissues treated with ROCK was sparser than the others, confirming that ROCK efficiently inhibited the growth of HCT-116 colorectal cancer. Moreover, Ki-67 immunohistochemical staining (IHC) showed that the number of positive tumor cells of the ROCK group prominently declined in comparison with others (Figs. 4G and H). The proliferation of tumor cells in ROCK group was the most slumber that further proved the antitumor activity of ROCK. These results validated that ROCK was extremely efficient gene delivery system and could resoundingly deliver pPAL to tumor tissues for the expression of PAL to deprive Phe only in HCT-116 cells to treat HCT-116 colorectal cancer.

Harnessing tumor cell microenvironment controlling design, the ROCK could diminish the side effects. Even though ROCK was administered systemically several times and over a long period, the body weight in the ROCK group of the mice did not show significant changes during the treatment period. The "locked" state of ROCK during blood circulation removed systemic toxicity (Fig. S7A in Supporting information) and normal organs (Fig. S7B in Supporting information). Safe and biodegradable nanocomplexes with precisely depriving intratumoral Phe will be further investigated for biomedical applications.

In summary, our developed ROCK could self-supply PAL and sustainably deprive Phe only in tumor cells, which caused the hindrance of tumor growth without systemic toxicity. Interestingly, the self-supply of PAL was not stopped until the tumor cell death. ROCK exhibited higher transfection, lower toxicity, and more effective endosomal/lysosomal escape compared with commercial transfection agent PEI 25 K. Our strategy selectively targeted Phe in tumor cells and was safer than traditional Phe deprivation. It was more thorough than non-EAAs deprivation, in which deprived non-EAAs could be obtained from compensatory mechanisms. Inflammation did not occur after intravenous injection of our nanocomplexes, indicating that our strategy overcame the problem caused by the immunogenicity of PAL. This pleasing result was owed to the programmable double-unlock property of ROCK. Therefore, we believed that the precise deprivation of important substances involved in metabolism is an important tumor treatment approach, and our gene delivery nanocomplex can be widely applied to cancer gene therapy.

## Declaration of competing interest

The authors declare that they have no known competing financial interests or personal relationships that could have appeared to influence the work reported in this paper.

## Acknowledgments

This work was financially supported by funds of Sichuan Province for Distinguished Young Scholar (No. 2021JDJQ0037) and the National Natural Science Foundation of China (No. 82172094).

## Supplementary materials

Supplementary material associated with this article can be found, in the online version, at doi:10.1016/j.cclet.2023.109275.

## References

[1] M. Butler, L.T. van der Meer, F.N. van Leeuwen, Trends Endocrinol. Metab. 32 (2021) 367–381.
[2] M.T. Kuo, H.H.W. Chen, L.G. Feun, et al., Pharmaceuticals 14 (2021) 72.
[3] S.E. LeBoeuf, W.L. Wu, T.R. Karakousi, et al., Cell Metab. 31 (2020) 339–350.
[4] E.L. Lieu, T. Nguyen, S. Rhyne, et al., Exp. Mol. Med. 52 (2020) 15–30.
[5] H. Rubin, Proc. Nat. Acad. Sci. U. S. A. 116 (2019) 6964–6968.
[6] M. Bacci, N. Lorito, L. Ippolito, et al., Cell Rep. 28 (2019) 104–118.
[7] A.K. Najumudeen, F. Ceteci, S.K. Fey, et al., Nat. Genet. 53 (2021) 16–26.
[8] S.V. Pokrovsky, E.O. Chepikova, Z.D. Davydov, et al., Curr. Med. Chem. 26 (2019) 446–464.
[9] K. Ramani, A.E. Robinson, J. Berlind, et al., Hepatology 75 (2022) 280–296.
[10] L. Kou, R. Sun, S. Xiao, et al., ACS Appl. Mater. Interfaces 11 (2019) 26722–26730.
[11] S. Li, W. Su, H. Wu, et al., Nat. Biomed. Eng. 4 (2020) 704–716.
[12] C. Liang, X. Yan, R. Zhang, et al., J. Control. Release 317 (2020) 109–117.
[13] W. Xu, H. Yang, Y. Liu, et al., Cancer Cell 19 (2011) 17–30.
[14] M. Uriarte, N. Sen Nkwe, R. Tremblay, et al., Nat. Commun. 12 (2021) 6984.
[15] J.S. Kang, Nutr. Metab. 17 (2020) 20.
[16] A.R. Moss, R. Schoenheimer, J. Biol. Chem. 135 (1940) 415–429.
[17] L.L. Moldawer, I. Kawamura, B.R. Bistrian, et al., Biochem. J. 210 (1983) 811–817.
[18] J. Yang, R. Tao, L. Wang, et al., J. Biomed. Nanotechnol. 15 (2019) 717–727.
[19] O.O. Babich, V.S. Pokrovsky, N.Y. Anisimova, et al., Biotechnol. Appl. Biochem. 60 (2013) 316–322.
[20] P.H.D. Nguyen, M.K. Jayasinghe, A.H. Le, et al., ACS Nano 17 (2023) 5187–5210.
[21] X. Li, R. Luo, X. Liang, et al., Chin. Chem. Lett. 33 (2022) 2213–2230.
[22] L. Li, L. Song, X. Liu, et al., ACS Nano 11 (2017) 95–111.
[23] N. Wang, C. Liu, Z. Lu, et al., Adv. Funct. Mater. 30 (2020) 2004940.
[24] X. Song, C. Liu, N. Wang, et al., Adv. Drug Deliv. Rev. 168 (2021) 158–180.
[25] S. Yang, C. Ou, L. Wang, et al., J. Control. Release 320 (2020) 253–264.
[26] R. Mohammadinejad, A. Dehshahri, V. Sagar Madamsetty, et al., J. Control. Release 325 (2020) 249–275.
[27] H. Lv, S. Ma, Z. Wang, et al., Chin. Chem. Lett. 32 (2021) 1765–1769.
[28] Y. Kuang, K. Zhang, Y. Cao, et al., ACS Appl. Mater. Interfaces 9 (2017) 12217–12226.
[29] L. Zhong, L. Xu, Y. Liu, et al., Acta Pharm. Sin. B 9 (2019) 397–409.
[30] X. Song, R. Wang, J. Gao, et al., Chin. Chem. Lett. 33 (2022) 1567–1571.
[31] K.N. Sugahara, T. Teesalu, P.P. Karmali, et al., Science 328 (2010) 1031–1035.
[32] L. Simón-Gracia, H. Hunt, P. Scodeller, et al., Biomaterials 104 (2016) 247–257.
[33] Y. Hao, Y. Chen, X. He, et al., Biomaterials 293 (2023) 121975.